Unclassified

SECURITY CLASSIFICATION OF THIS PAGE

REPORT DOCUMENTATION PAGE

Form Approved OMB No. 0704-0188

1a AD-A235 288

2a

2b

1b. RESTRICTIVE MARKINGS

3. DISTRIBUTION/AVAILABILITY OF REPORT
Approved for public release; Distribution unlimited

4. PERFORMING ORGANIZATION REPORT NUMBER(S)
PL-TR-91-2081

5. MONITORING ORGANIZATION REPORT NUMBER(S)

6a. NAME OF PERFORMING ORGANIZATION
Phillips Lab, Geophysics Directorate

6b. OFFICE SYMBOL (If applicable)
PHG

7a. NAME OF MONITORING ORGANIZATION

6c. ADDRESS (City, State, and ZIP Code)
Hanscom AFB
Massachusetts 01731-5000

7b. ADDRESS (City, State, and ZIP Code)

8a. NAME OF FUNDING/SPONSORING ORGANIZATION

8b. OFFICE SYMBOL (If applicable)

9. PROCUREMENT INSTRUMENT IDENTIFICATION NUMBER

8c. ADDRESS (City, State, and ZIP Code)

10. SOURCE OF FUNDING NUMBERS

PROGRAM ELEMENT NO	PROJECT NO	TASK NO	WORK UNIT ACCESSION NO
61102F	2311	G5	02

11. TITLE (Include Security Classification)
Electric Field Measurements During Supercharging Events on the MAIMIK Rocket Experiment

12. PERSONAL AUTHOR(S)
W.F. Denig, N.C. Maynard, W.J. Burke, B.N. Maehlum*

13a. TYPE OF REPORT	13b. TIME COVERED	14. DATE OF REPORT (Year, Month, Day)	15. PAGE COUNT
Reprint	FROM _____ TO _____	1991 April 23	10

16. SUPPLEMENTARY NOTATION *Norwegian Defense Research Establishment, Kjeller, Norway
Reprinted from Journal of Geophysical Research, Vol. 96, No. A3, pp 3601-3610, March 1, 1991

17. COSATI CODES		
FIELD	GROUP	SUB-GROUP

18. SUBJECT TERMS (Continue on reverse if necessary and identify by block number)
Active space experiments, Electron beams, Electric fields

19. ABSTRACT

We report on the observation and analysis of quasi-DC electric fields measured during active electron emission from the MAIMIK sounding rocket. The MAIMIK mother-daughter tethered rocket consisted of two separately instrumented payload sections which were detached in-flight. The daughter payload included a variable current, 8-keV electron accelerator and instrumentation to measure the vehicle potential relative to the ionospheric plasma. The electric field detector was part of the quiescent mother payload which separated from the daughter at a constant speed. Of particular interest to the present study were the observations of impulsive electric fields measured at the initiation of the beam for emission currents which drove the daughter payload into an overcharged state. At locations well removed from the active payload the electric field signature consisted of a 1- to 2-ms, monopolar impulse field that had a rapid risetime and a more gradual decay. The components of the vector field were examined using a cylindrical coordinate system that placed the active payload at the origin and fixed the azimuthal injection angle of the beam. In general, the radial components of the field were directed out from the positively charged central body and presumed to be of electrostatic origin. The tangential components had consistent positive deflections indicating that these field components were mostly electromagnetic in nature. We suggest that the measured impulse fields were due to a shielded ion blast wave propagating away from the highly charged central body with azimuthal asymmetries created by the distribution of space charge associated with a virtual cathode and escaping beam electrons. The time-varying electrostatic fields drove transient Hall currents that were carried by cold electrons $\mathbf{E} \times \mathbf{B}$ drifting near the head of the blast wave.

DTIC ELECTE MAY 06 1991 S E D

20. DISTRIBUTION/AVAILABILITY OF ABSTRACT
☐ UNCLASSIFIED/UNLIMITED ☒ SAME AS RPT. ☐ DTIC USERS

21. ABSTRACT SECURITY CLASSIFICATION
Unclassified

22a. NAME OF RESPONSIBLE INDIVIDUAL	22b. TELEPHONE (Include Area Code)	22c. OFFICE SYMBOL
W.F. Denig	(617) 377-2431	PHG

DD Form 1473, JUN 86 Previous editions are obsolete. SECURITY CLASSIFICATION OF THIS PAGE

Unclassified

JOURNAL OF GEOPHYSICAL RESEARCH, VOL. 96, NO. A3, PAGES 3601-3610, MARCH 1, 1991

Electric Field Measurements During Supercharging Events on the MAIMIK Rocket Experiment

W. F. DENIG, N. C. MAYNARD, AND W. J. BURKE

Geophysics Laboratory, Hanscom Air Force Base, Bedford, Massachusetts

B. N. MAEHLUM

Norwegian Defence Research Establishment, Kjeller, Norway

We report on the observation and analysis of quasi-DC electric fields measured during active electron emission from the MAIMIK sounding rocket. The MAIMIK mother-daughter tethered rocket consisted of two separately instrumented payload sections which were detached in-flight. The daughter payload included a variable current, 8-keV electron accelerator and instrumentation to measure the vehicle potential relative to the ionospheric plasma. The electric field detector was part of the quiescent mother payload which separated from the daughter at a constant speed. Of particular interest to the present study were the observations of impulsive electric fields measured at the initiation of the beam for emission currents which drove the daughter payload into an overcharged state. At locations well removed from the active payload the electric field signature consisted of a 1- to 2-ms, monopolar impulse field that had a rapid risetime and a more gradual decay. The components of the vector field were examined using a cylindrical coordinate system that placed the active payload at the origin and fixed the azimuthal injection angle of the beam. In general, the radial components of the field were directed out from the positively charged central body and presumed to be of electrostatic origin. The tangential components had consistent positive deflections indicating that these field components were mostly electromagnetic in nature. We suggest that the measured impulse fields were due to a shielded ion blast wave propagating away from the highly charged central body with azimuthal asymmetries created by the distribution of space charge associated with a virtual cathode and escaping beam electrons. The time-varying electrostatic fields drove transient Hall currents that were carried by cold electrons $\mathbf{E} \times \mathbf{B}$ drifting near the head of the blast wave.

INTRODUCTION

Over the past 20 years rocket-borne electron accelerators in the ionosphere have been used to produce artificial aurora, to act as geomagnetic field line-tracers, and to actively perturb the local plasma environment (see reviews by *Winckler* [1980], *Szuszczewicz* [1985], and *Maehlum* [1988]). The limited ability of the local ionospheric plasma to neutralize the emitted charge was a major concern of these early rocket experimenters [*Parker and Murphy*, 1967; *Hess et al.* 1971, *Hendrickson et al.*, 1971]. They feared that the electrical charging of the host vehicle relative to the local ionospheric plasma would degrade the effective power of the emitted beam. Experience soon showed, however, that these concerns were largely unfounded. Emitted electron beams were relatively unaffected by spacecraft that, for the most part, acquired low levels of charging. These seemingly anomalous results were explained by invoking a strong coupling between the beam and the background plasma resulting in enhanced ionization of the background neutral gas and an increase in the return current flux [*Cambou et al.*, 1975]. Further investigations of this coupling mechanism have led to an increased understanding of the fundamental interactions between a beam system and the ionospheric plasma [see *Grandal*, 1982].

Recently, a number of investigators have reported on ionospheric experiments in which significant vehicle charging occurred during active electron emission [*Jacobsen and Maynard*, 1980; *Winckler et al.*, 1989; *Myers et al.*, 1989]. There have also been reports of vehicle charging in excess of beam energies [*Managadze et al.*, 1988; *Maehlum et al.*, 1988], a phenomenon which has been referred to as the overcharged or supercharged state. *Maehlum et al.* [1988] have suggested that the conditions responsible for the overcharging of the MAIMIK rocket payload were the high beam-to-plasma density ratio and the small current collecting area of the emitting vehicle. A theoretical understanding of the overcharging phenomenon is currently emerging [*Winglee and Pritchett*, 1988; *Mandell et al.*, 1988; *Singh and Hwang*, 1989]. A key element common to these theories is the formation of a virtual cathode near the gun aperture. The negative space charge of the cathode reflects a fraction of the primary beam back to the vehicle but permits the remainder of the beam to be transmitted. The escaping charge sustains the mechanism [*Miller*, 1982] and provides the means for the vehicle overcharging.

The overcharging condition arises from complex interactions between the charged vehicle, the virtual cathode, and the ambient plasma. A natural consequence of overcharged space vehicles is the formation of high-potential sheaths which evolve in time to shield the remote plasma from the charged body. High-potential sheaths differ from classical Debye sheaths in both the magnitudes of the potential gradients and their spatial extent.

The temporal evolutions of the electron and ion sheath components operate on the respective time scales of the electron and ion plasma oscillation periods [*Borovsky*, 1988]. In the ionosphere these times can vary from a fraction of a microsecond to greater than a millisecond. It is generally believed that the quasi-static sheaths that surround highly

Paper number 90JA02103.
0148-0227/91/90JA-02103$05.00

charged space vehicles involve three distinct regions: (1) a near-source region of large potential gradients where charge neutrality is strongly violated, (2) an intermediate, quasi-neutral region of reduced electric fields, and (3) a distant region where the ambient plasma is well shielded [*Cooke and Katz*, 1988]. The complex nature and the large range of time scales involved in the formation of the high-potential sheath structures are difficult to study both analytically and through computer simulations.

There exists only a limited amount of data available to test our understanding of high potential sheaths for space experiments using active electron emission. *Myers et al.* [1989] have compared the steady-state current collection characteristics for highly charged bodies both with and without electron beams for the Cooperative High Altitude Rocket Gun Experiment (CHARGE) 2. Although the nonemission cases compared well with the *Parker and Murphy* [1967] sheath theory, the measured return currents during beam emissions greatly exceeded the model predictions. *Myers et al.* [1990] also measured the transient response of the potential for the CHARGE 2 rocket at the start of the beam. The initial risetime for the vehicle's potential was measured to be of the order of 10 μs, whereas steady state conditions were achieved of the order of 1 ms. *Kellogg and Monson* [1988] reported the observation of energetic ions during the Some Compatible Experiments (SCEX) 2 rocket that were consistent with an initial rapid acceleration of the background plasma around the charged payload. Onset electric fields, detected at the start of the beams, were measured during the POLAR 5 [*Jacobsen and Maynard*, 1980] and ECHO 6 [*Erickson and Winckler*, 1988] rocket experiments. These authors interpreted their individual results in terms of a charged central body and the temporal responses for sheath formation. *Maynard et al.* [1982] determined from the POLAR 5 onset field measurements that the shielding time for the beam-emitting payload was several milliseconds. Of particular note for the POLAR 5 and ECHO 6 experiments was the absence of electric field signatures at the termination of the beams.

Here we report on measurements relevant to the evolution of electric field structures near the MAIMIK sounding rocket during times when the beam-emitting payload was in an overcharged state. Results of previous MAIMIK analyses reported by *Maehlum et al.* [1988, 1990] and *Svenes et al.* [1988] are incorporated into the present study. The relevant portions of the MAIMIK rocket are described in the next section, followed by a presentation of the MAIMIK electric field data. Our analyses of the E field data indicated that the temporal behavior of the fields was consistent with ion responses to the rapid charging of the active payload. Spikelike electric fields at the initiation of the gun pulse were found to have both electrostatic and electromagnetic components. The electrostatic variations reflected the dynamics of the ion expulsion from the inner sheath and the shielding of the ion blast wave. The electromagnetic components were driven by time-varying Hall currents carried by $\mathbf{E} \times \mathbf{B}$ drifting electrons. In order to address some of the shortcomings of the blast wave model a vacuum solution is presented that has only a limited applicability on the time scale of the MAIMIK measurements but may introduce asymmetries in the distribution of charges within the sheath and expanding ion blast wave that help explain the data. The discussion section is followed by our concluding remarks.

INSTRUMENTATION

The MAIMIK sounding rocket was launched in a northwesterly direction into a quiet subauroral ionosphere at 1856 UT on November 10, 1985, from the Andoya Rocket Range (69°17′39″ N, 16°01′15″ E) in northern Scandinavia. The payload section of the Terrier/Black Brant two-stage vehicle consisted of separate mother and daughter payloads that were detached 62 s after launch with the aft-mounted mother remaining attached to the second-stage motor. Thereafter, the separation velocity of the daughter relative to the mother payload was a constant 0.8 m s^{-1} at 23° to the local magnetic field. Attitude stability for both the mother and daughter payloads was maintained by their respective spins of 0.3 Hz and 3.3 Hz. The coning half-angle for the mother was 35° with a coning period of 300 s. The coning half-angle for the daughter was much less severe, being about 5°. The MAIMIK payloads achieved an apogee of 381 km at 320 s after launch.

During the interval between separation and 113 s, the mother and daughter payloads were electrically tethered through a 10 MΩ impedance. This time interval overlapped the initial electron beam operations which commenced at 101 s and continued throughout the remainder of the flight. The purpose of the tether was to provide a "mother" ground reference during the electron beam pulses when the daughter was actively charged relative to the background plasma. Although the mission plan was to keep the two payloads tethered until 130 s, the premature disconnection of the tether wire at 113 s limited the total amount of tether data available.

Figure 1 is a simplified schematic of the MAIMIK rocket payload detailing the instrument geometry for several of the experiments relevant to the present study. Included as part of the daughter payload were the electron accelerator, a set of electron retarding potential analyzers, and a tether volt-

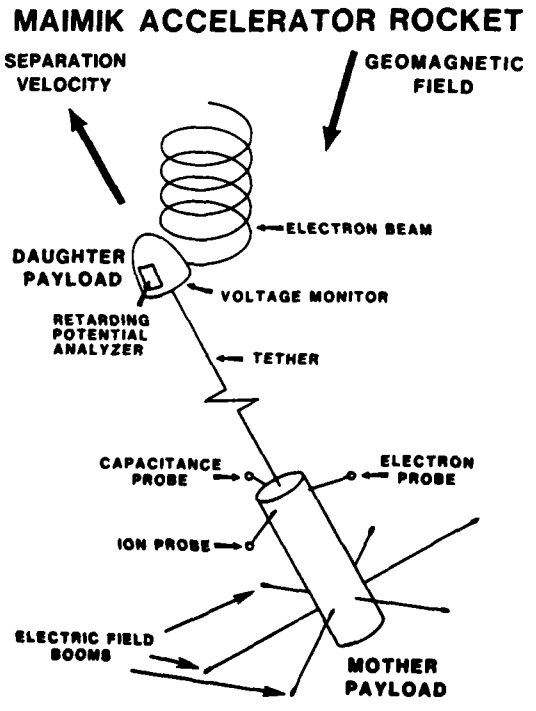

Fig. 1. Schematic representation of the MAIMIK mother and daughter payloads.

age monitor. The retarding potential analyzers provided an alternate means of monitoring the daughter's voltage by measuring the differential electron energy flux to the payload within an energy range from ~0 eV to -3.2 keV relative to daughter ground. The daughter also had a magnetometer that was used to determine the beam injection pitch angle and the vehicle's attitude with a time resolution of 3.3 ms. The instrument complement on the mother included a set of plasma probes, a set of three-axis electric field probes, a three-axis gyro system, and a magnetometer. The boom-mounted plasma instrumentation consisted of a sweeping Langmuir probe, a capacitance probe, and an ion probe. Data from the mother's gyro and magnetometer were used to calculate an instantaneous attitude for the vehicle with a time resolution of 3.3 ms. The electric field instrument and the electron accelerator are described in more detail below. Further information regarding the MAIMIK rocket and its flight performance can be found in an overview paper by *Maehlum et al.* [1987]. The charging characteristics of the active payload and the response of the local plasma to the beam interaction have been described previously by *Maehlum et al.* [1988, 1990] and *Svenes et al.* [1988]. A study of ram and wake effects during nonbeam periods has also been recently published [*Svenes et al.*, 1990].

The electron accelerator system on the daughter payload consisted of a set of five identical gun units each operating in an emission-limited diode configuration with a fixed accelerator voltage of 8 keV [*Syvertsen*, 1985]. The gun heads were designed with a 5-mm aperture and a perveance of 3.2×10^{-7} A $V^{-3/2}$. Sequential 11-ms pulses of 320 mA, 80 mA, 40 mA, 20 mA, 40 mA, 80 mA, 160 mA, and 800 mA were injected into the ionosphere at a pulse repetition frequency of 1.2 Hz. For currents in the range 20 mA to 160 mA only a single gun head was used to generate the beam. The 320 mA and 800 mA current pulses required the simultaneous operation of two and five heads, respectively. The nearly DC beam operated at a high-voltage chopper frequency of 1.2 kHz with a voltage ripple of less than 2 kV below the nominal accelerator voltage. During the MAIMIK flight the injection pitch angles for the unfocused beam ranged from 65° to 115° with a half-angle beam spread of about 10°. Although the electron gun was instrumented to monitor accelerator voltages and currents these data channels were carried by a telemetry system that failed early in the flight. The values used in the present analysis were from preflight calibrations.

Vector electric fields at the location of the MAIMIK mother payload were measured using an orthogonal, three-axis set of double probes. Each double probe consisted of a boom pair having 61-cm-long cylindrical elements at the extremes that contacted the plasma and whose potential was monitored through a 10^{12} Ω preamplifier impedance and referenced to the rocket body. The inner portion of each boom was insulated from the plasma by a coating of Kapton. As depicted in Figure 1, two of the boom pairs were mounted at 45° to the rocket spin axis while the third pair was in a plane perpendicular to the spin axis. The 45° booms were constructed of rigid stainless steel whose active elements had a nominal separation of 5.7 m. The pair in the spin plan had a separation length of 8.8 m and were fabricated using a flexible beryllium-copper alloy. The electric field booms were deployed between 70 s and 100 s.

The components of the local electric field were derived in a straightforward fashion as the negative of the potential difference between each boom pair divided by the boom length. The sensitivity of the vector instrument ranged from 3 mV m^{-1} (limited by the 8-bit telemetry system) to greater than 1 V m^{-1}. The measurements were corrected for motion-induced electric fields and for contact potential variations. A careful analysis was made to avoid the use of data that had been adversely affected by possible geometric effects [*Bering*, 1983] and severe plasma density or temperature gradients [*Steinberg et al.*, 1988]. A determination of the statistical errors associated with the steady state electric field measurements was made by monitoring the ambient ionospheric field between successive beam pulses. These errors were calculated to be no greater than ±5 mV m^{-1}.

As a general comment we note that the rapid temporal responses to electron beam injections were near the limit of the rocket telemetry system. The fast rise in the daughter's potential at the initiation of the gun pulse was measured with the tether voltage monitor and the retarding potential analyzers. The nominal sampling frequencies for these instruments were 3.7 kHz and 2.4 kHz, respectively. The measured daughter potential at beam initiation for the larger currents was instantaneous on these time scales [*Maehlum et al.*, 1988, Figure 2]. On the other hand, the daughter's potential for the smaller current beams increased more slowly and could be measured. Although this trend continued throughout the remainder of the flight, the effects of the smaller currents were not of primary interest here.

Perhaps of even greater concern was the effect that a rapidly changing electric field had on the measurements made by the mother payload. We note that although the vector instrument had a telemetry frequency of 2.5 kHz, within each sampling period the three components of the field were measured sequentially with a 0.1-ms separation between the x and y boom axes and the y and z boom axes. This telemetry sampling format tended to prejudice the data for rapidly varying fields. Cognizant of this limitation, the measured vector response for each beam pulse was examined for possible aliasing effects. In general, this was not a serious problem for the determination of the vector orientation of the measured fields but did limit the instrument's ability to detect the maximum amplitude of spikelike fields. This topic will be considered in more detail in the following section.

ELECTRIC FIELD MEASUREMENTS

Electric fields in the vicinity of the mother payload measured continuously throughout the MAIMIK rocket flight were superpositions of the ambient ionospheric electric fields and the beam-pulse responses. Prior to 340 s the background field was near zero and within the ±5 mV m^{-1} accuracy of the measurements. The geomagnetic northward component of the field gradually increased to 30 mV m^{-1} near 340 s when the northwest traveling rocket was located near a corrected geomagnetic latitude of 67° and 21.2 MLT. These background measurements suggest that at the time of this transition the MAIMIK rocket crossed the equatorward boundary of the auroral zone. All the beam-induced electric field measurements that are discussed here were made in the subauroral ionosphere.

The present analysis is an examination of the electric field characteristics measured at the locations of the mother during electron beam operations on the daughter. Several typical examples of the uncorrected field signatures for 160-mA beam emissions are shown in Figure 2. The legend accom-

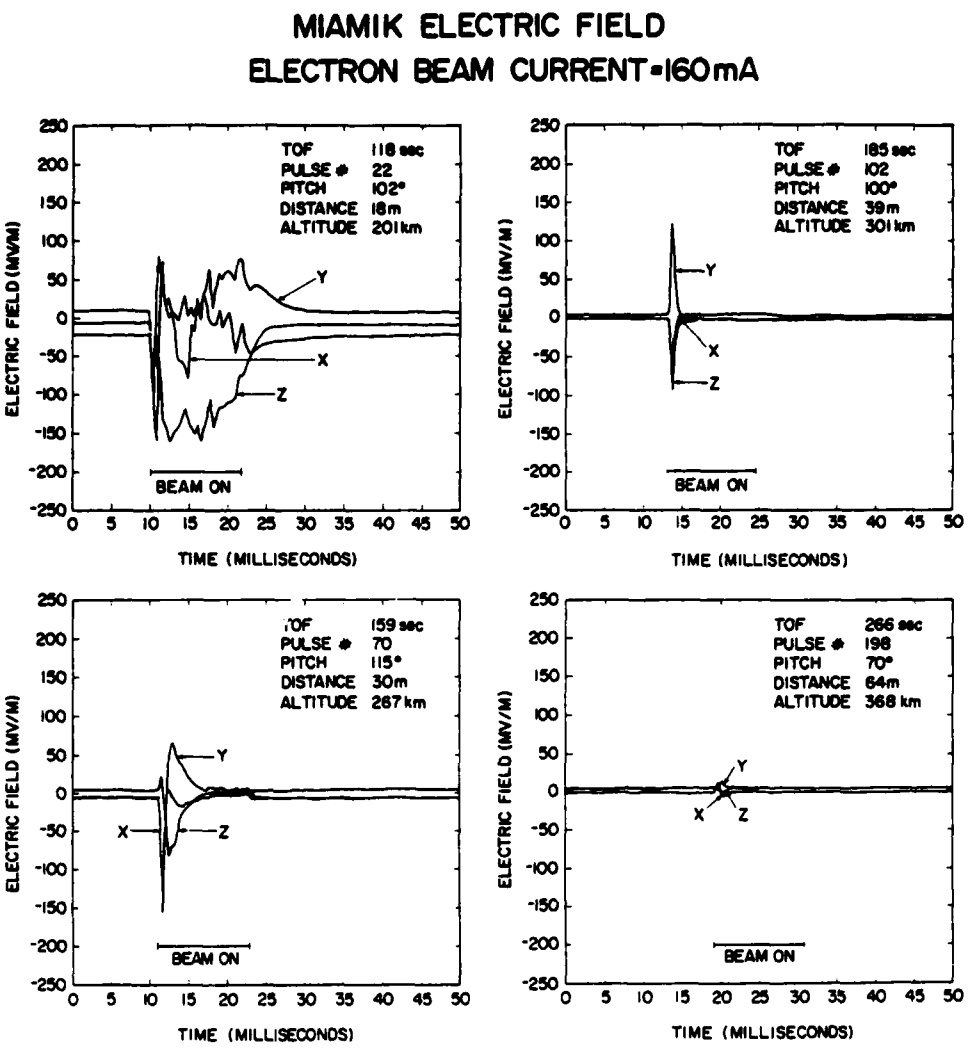

Fig. 2. Four examples of uncorrected electric field measurements for 160-mA beam operations. The injection pitch angle, the perpendicular separations of the payload, and the altitude are noted.

panying each beam pulse specifies the time of flight (TOF), the pulse number, the injection pitch angle, the mother-daughter cross-field separation, and the altitude. The clear differences in the pulse signatures for this current level were mostly due to the increasing separation between the payloads. Within a 30-m cross-field separation the electric field response was a combination of an initial impulse lasting up to several milliseconds and an often complicated long-lived field persisting at least the entire 11-ms gun pulse. Beam aftereffects were also detected within the disturbed plasma region near the daughter. The character of the pulse signature changed near 30 m with the persistent fields becoming less intense and leaving only an initial impulse response as evidence of the beam. The impulse fields were the prevalent beam responses measured in the interval between 30 m and 65 m. Beyond about 65 m the amplitude of the impulse field fell below the sensitivity of the instrument.

Electric field signatures during the 320-mA and 800-mA current emissions were qualitatively similar to the set of 160-mA beam pulses presented in Figure 2. Quite distinct, however, were the signatures for the 40-mA beams that had only a weak persistent field within the 30-m cross-field region and never produced an initial impulse response. On the other hand, the pulse signatures for the 80-mA currents produced mixed results and lacked the consistency found at both the higher and lower currents. For example, there was, at times, evidence for both initial spikelike fields and persistent fields within the 65-m cross-field range. Finally, the 20-mA beam pulses produced no significant fields at any separation distance.

A detailed examination of the impulse field response for the larger currents indicated that the electric fields were monopolar with risetimes greater than about 0.3 ms and falloffs of about 1- to 2-ms. Figure 3 is a plot of the measured components of the field for a typical pulse response and a set of simple curves used to illustrate the impulse signature. The data plotted in the figure were acquired during a 160-mA beam emission at a cross-field separation of 45 m. The offset in the start of the measured pulse response is relative to the last unperturbed sample interval and is not intended to represent the delay time between beam initiation and the remote field response. The response curve for each vector component was approximated as a linearly increasing function and an exponentially decreasing function with an e-folding decay time of 0.35 ms. Note that the individual data points illustrate the limitation posed by the

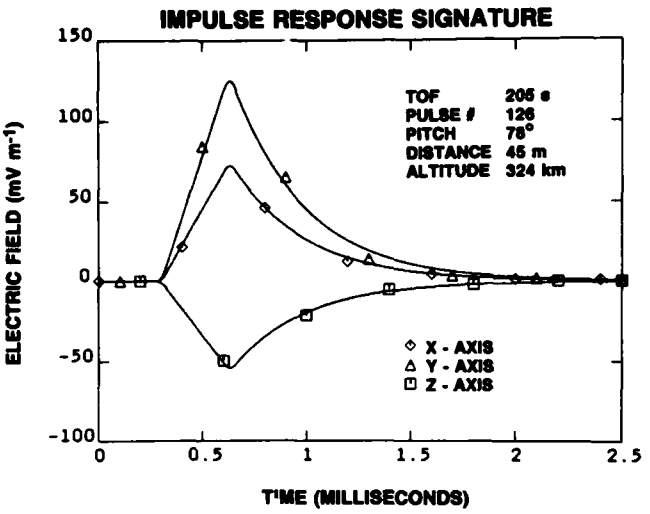

Fig. 3. Typical electric field impulse response measured at the initiation of an 11-ms beam pulse. The time scale was set by the telemetry sampling interval and was not specifically correlated with the start of the beam pulse.

telemetry sample rates. For example, the curves in Figure 3 include a 0.1- to 0.2-ms uncertainty in the location of the peak field during which time the magnitude of the vector might have varied by a factor of 2. The sampling format for the three-axis measurements also introduced a slight error ($\leq 15°$) in the orientation of the impulse fields. The electric field vectors presented in the remainder of this section were formed from the sequentially measured boom components within one telemetry sampling period and were subject to the errors discussed here.

Figure 4 is a summary plot of the initial pulse responses measured within the cross-field separation range from 30 m to 60 m. The electric field data have been corrected and plotted in a local geomagnetic coordinate system. Included on the plot are the beam currents and injection pitch angles. At the time of these measurements the active daughter was positioned north (positive x), west (negative y), and up (opposite to $\mathbf{B}$) relative to the mother payload. The summary data indicate that the perpendicular electric field responses for the 160-mA and larger beam currents were qualitatively similar in that the perpendicular projections of the field pointed toward the southeast and generally away from the active vehicle. On the other hand, the z components pointed up towards the daughter between 165 s and 215 s but gradually turned downwards at larger distances.

In order to present a synoptic view of the perpendicular projections for the impulse electric fields a field-aligned cylindrical coordinate system has been adopted that places the active daughter at the origin and fixes the azimuthal injection angle of the beam. Figure 5 is a summary plot of the impulse fields for the 160-mA, 320-mA, and 800-mA currents. The different current levels have been identified by the symbols at the base of the vectors. The nominal trajectory of the 8-keV electron beam injected along the positive ordinate axis had a clockwise rotation and a gyrodiameter of 12 m, as indicated. Due to the increasing mother-daughter separation and the spin of the beam-emitting payload the locus of points representing the mother's locations traced out a separate spiral of increasing radii for each beam current. The advantage of this coordinate system is the clarity that it allows for representing the full set of field data on a single plot where the source of the disturbance was fixed at the origin. The field-aligned components have not been replotted from Figure 4 since these vector components were not affected by the transformation.

Figure 5 shows that the perpendicular electric field responses to the electron beams consisted of outward pointing radial components and tangential components. The set of field measurements shows a significant azimuthal variation in the amplitudes of the radial components that were greater than the uncertainty in the measurement. We suspect that

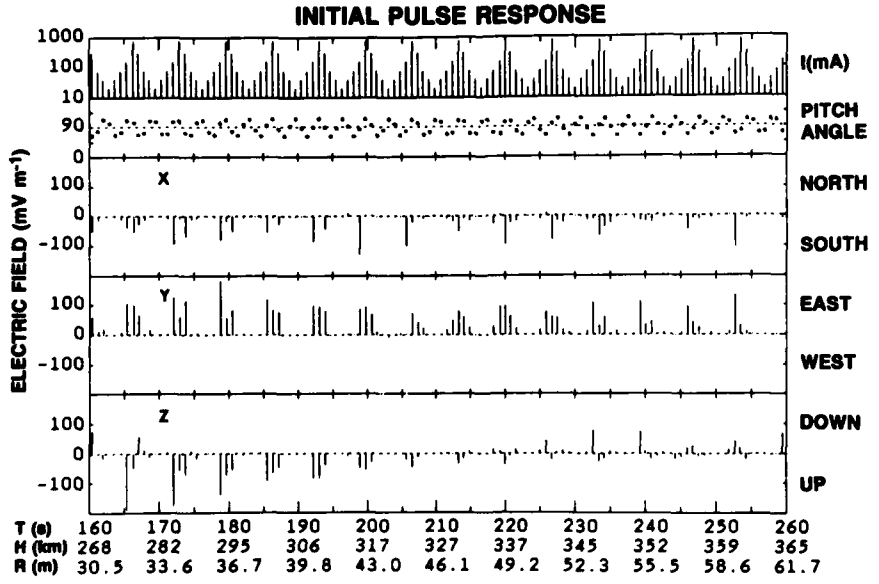

Fig. 4. Survey plot of the impulse field responses to beams of all currents detected within the cross-field range from 30 m to 60 m. The data are presented in a fixed geomagnetic coordinate system with an active payload located to the northwest and upwards relative to the mother. The beam currents and injection pitch angles are indicated in the top two panels.

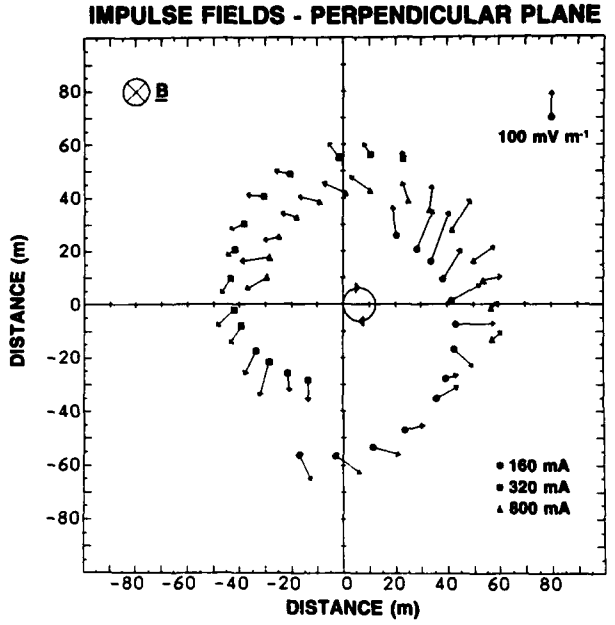

Fig. 5. Survey plot of the perpendicular components of the measured impulse electric fields for beam emissions of 160 mA, 320 mA, and 800 mA. The data are presented in a coordinate system that places the daughter at the origin and fixes the azimuthal injection angle of the electron beam as shown.

the radial components were mostly the electrostatic fields due to the partial shielding of the inner space charge and that the initial space charge distribution near the daughter payload caused the observed amplitude variations. On the other hand, the consistent counterclockwise deflection in the outward fields suggests that $\oint \mathbf{E} \cdot \mathbf{dl} \neq \mathbf{0}$ or, equivalently, that the tangential components were mostly of electromagnetic origin. The similar time responses for the radial and tangential components further suggest that they were responding to the same driving source.

DISCUSSION

The MAIMIK electric field data have provided us with a glimpse of the dynamic plasma processes occurring near the active daughter payload during electron beam operations. We have developed a qualitative model of the interaction between the active payload and the ambient plasma background that is consistent with some of the more salient features of the measured fields. Although this model was developed to explain the electric field data, including the apparent causal relationship between the radial and tangential impulse components, it was also important for us to consider how the model could be integrated into the overall picture that has evolved for the MAIMIK supercharging phenomenon reported by *Maehlum et al.* [1988] and the anomalous plasma heating results discussed by *Svenes et al.* [1988]. Cognizant of this consideration, we have strived to present an interpretation of the interaction that is both physically plausible and consistent with the full MAIMIK data set.

One of the more intriguing aspects of the MAIMIK experiment was the supercharging of the daughter payload during active electron beam emissions. As previously noted, *Maehlum et al.* [1988] speculated that the mechanism responsible for supercharging was the formation of a virtual cathode near the payload section. The negative space charge potential of the virtual cathode reflected a fraction of the primary beam back to the spacecraft. It also thermalized some of the beam particles to energies greater than the potential barrier of the cathode. This transmitted portion of the beam provided the means for the vehicle to supercharge.

As an initial attempt to understand the MAIMIK electric field measurements and to determine the constraints which set the upper bound on the radial electric field we calculated a vacuum solution to Poison's equation for a charged conducting body in the presence of a space charge distribution [*Maehlum et al.*, 1990]. The potential of the active vehicle was set at 14 keV in accordance with the MAIMIK tether measurements [*Maehlum et al.*, 1988]. In addition to the dominant effect of the positively charged vehicle, the presence of a virtual cathode and the excess charge created by the escaping beam were approximated by a Gaussian-distributed negative line charge aligned with the magnetic field. In our earlier work [*Maehlum et al.*, 1990] we added an ad hoc positive line charge beyond the virtual cathode that within a limited azimuthal range, improved the comparison between the orientation of the perpendicular electric field components in the model and the set of MAIMIK measurements for the 160-mA beam emissions. Since we had no physical explanation for this positive charge and since it did not adequately solve the problem, we have eliminated it here. Figure 6 includes plots of the measured electric fields for the 160-mA beams and the vacuum model results for a -3.50×10^{-7} C line charge (integrated) with an exponential density decay of 25 m. The cross-field location of the line charge is indicated in the top panel of Figure 6. This figure is a cross-sectional plot of the potential distribution in the plane perpendicular to $\mathbf{B}$ around the charged payload. The line charge was adjusted to provide the best directional (but not necessarily magnitude) fit to the data. These model results qualitatively show the dominant effect of the central body, the counterclockwise deflections of the perpendicular fields within a limited azimuthal range, and the reversal in the orientation of the field-aligned components of the electric fields. The model also allows for an azimuthal dependence in the magnitude of the radial component. Although similar techniques could be used to separately model the electric fields for the 320-mA and 800-mA beams, it is unlikely that such a simple distribution of space charge could model the full data set, particularly the $\oint \mathbf{E} \cdot \mathbf{dl} \neq \mathbf{0}$ tendency noted earlier. The vacuum model poses some additional problems related to the form of the impulse signature that will be discussed later. While it is particularly instructive in describing the instantaneous potential configuration near the active payload at beam turn-on, other processes are clearly necessary to represent the data.

In the tether voltage measurements of *Maehlum et al.* [1988] the authors noted a current threshold, near 80 mA, above which the supercharging phenomenon occurred. A similar threshold was also noted by *Svenes et al.* [1988] for the beam-induced electron heating rate of the ambient background plasma. The authors found that within a 30-m cross-field region about the active payload the calculated electron temperatures maximized for the 80-mA beams and decreased significantly for the larger currents. *Svenes et al.* [1988] attributed this effect to the reduced interaction length for the beam during vehicle supercharging when the bulk of the primary beam was reflected back to the rocket.

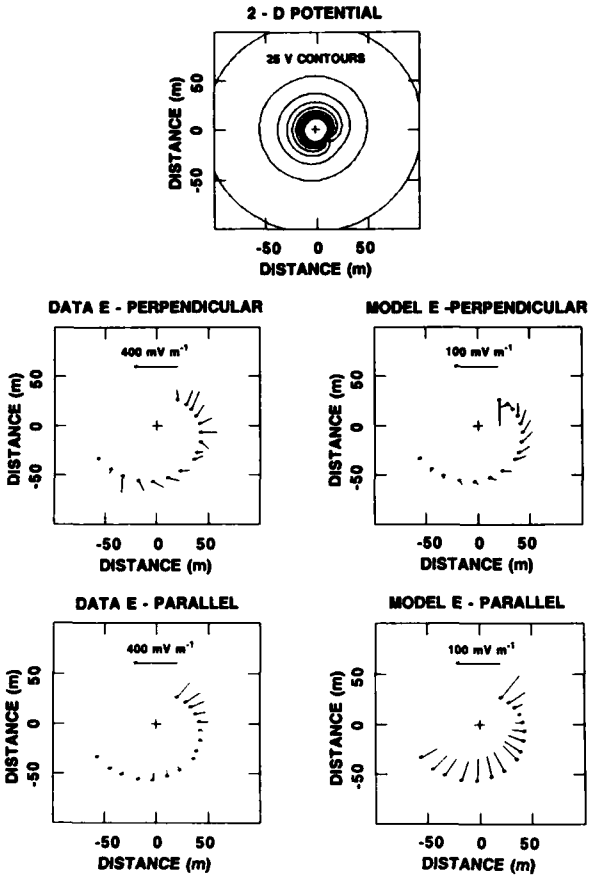

Fig. 6. MAIMIK vacuum model solution for a 14-keV conducting central body in the presence of a Gaussian distributed line charge of -3.25 × 10^{-7} C. The model electric fields and the measured electric fields for the 160-mA beams are presented for comparison (note difference in amplitude scale). The potential plot is in the plane perpendicular to **B** that contains the daughter while the model fields are calculated at the location of the mother. The field-aligned (parallel) electric field components are plotted with upward (downward) fields pointing in the outward (inward) radial direction.

It was noted in the last section that the impulse electric fields were consistently observed only for currents greater than 80 m, suggesting a common threshold value with the supercharging and plasma heating results. Unfortunately, the premature cutting of the tether prevented the unambiguous association of a unique threshold value for the simultaneous observations of (1) the supercharging phenomenon, (2) the decreased heating efficiency of the beam, and (3) the impulse field response. The combined data sets do suggest, however, that this simultaneity was real and represented a fundamental change in the beam-rocket-plasma system. We suggest that the high charging of the central body accelerated the local ions and created a blast wave propagating radially outward. This concept will be qualitatively developed below to particularly address the $\oint \mathbf{E} \cdot \mathbf{dl} \neq 0$ tendency noted earlier.

A distinct change in the electric field signatures was observed at the 30-m cross-field boundary where the intensity of the persistent field decreased leaving only the impulse fields as evidence of the beam. The limited radial extent of the persistent electric fields coincided with the heated plasma region reported by *Svenes et al.* [1988]. We suspect that this location corresponded to the outer boundary of the quasi-neutral sheath [*Cooke and Katz*, 1988] and that the complexity of the measured fields within the sheath was due to the combined effects of a partial shielded payload and gradients in the background temperature and density.

It is possible to estimate the radial size of the strong sheath region by assuming that the background ions were totally excluded from the inner sheath region and that residual electrons shielded the net space charge of the rocket. The surface area of the daughter can be approximated as a sphere of 30-cm radius with an equivalent vacuum capacitance of 33 pF. The net space charge of the rocket was estimated to be 4.6 × 10^{-7} C at the highest charging level of 14 keV. The equivalent charge radius for the inner sheath was therefore about 2.6 m for a background plasma density of 4 × 10^4 cm^{-3}.

It is germane to the present discussion to examine the typical plasma time scales and the dynamics of the electron and plasma sheaths near the active payload. Towards this end we have provided in Table 1 a short list of the characteristic plasma times appropriate for the MAIMIK experiment.

TABLE 1. Characteristic Frequencies and Periods

Mode	Frequency, Hz	Period, s
Electron plasma	1.8×10^6	5.6×10^{-7}
Electron cyclotron	1.4×10^6	7.1×10^{-7}
Ion plasma	1.0×10^4	1.0×10^{-4}
Lower hybrid	6.4×10^3	1.6×10^{-4}
Ion cyclotron	4.8×10^1	2.1×10^{-2}

An estimate of the vehicle charging rate was made by calculating the time required for the active payload to acquire an excess positive charge at the initiation of the gun pulse. Using the estimated value for the net space charge of the rocket, the charging time was determined to be of the order of 10 μs at the larger beam currents. The charging time was therefore significantly greater than the electron plasma period but less than the ion response. Consequently, we conclude that the electron gas could accommodate itself to the quickly changing daughter potential but that the massive local ions could not. These residual ions were accelerated by the strong electric fields and rapidly ejected from the inner sheath after beam turn-on.

The ions that were explosively ejected from the inner sheath had resultant speeds dependent upon their point of origin within the sheath. An ion originating deep within the sheath was assumed to have acquired a significant kinetic energy limited by the maximum charging level of the spacecraft. For example, an O^+ ion near the MAIMIK daughter acquired a kinetic energy of some 14 keV at the highest charging levels with a resultant speed of 4.1 x 10^5 m s^{-1}. Parts of the energetic ion cloud rapidly expanded across the sheath regions and into the undisturbed plasma on submillisecond time scales. Comparing these transit times with the electron and ion cyclotron periods listed in Table 1, we note that within the underlying system dynamics the background electrons were effectively magnetized but the ions were not. In other words, although the electrons within the sheath were effectively tied to the local magnetic field, the ion cloud freely expanded across it on the time scale of several milliseconds.

The observational characteristics of the MAIMIK electric field data that must be an integral part of the proposed model are the systematics of the impulsive electric field. Figure 7 is a schematic of the interaction model for the MAIMIK beam experiment where the emphasis has been placed on the transverse electric field; that is, the radial and tangential components. By way of introduction, the more salient features of the model are summarized before embarking on a more detailed analysis. Our basic contention is that the direct source of the radial components of the impulse fields was the net space charge of the expanding ion cloud in the regions beyond the strong inner sheath. These local electric fields caused the background electrons to initiate an $\mathbf{E} \times \mathbf{B}$ drift on time scales more rapid than the response time of the ions. The transient Hall currents $\mathbf{J_H}$ generated by the flowing electrons induced the tangential electric fields as measured.

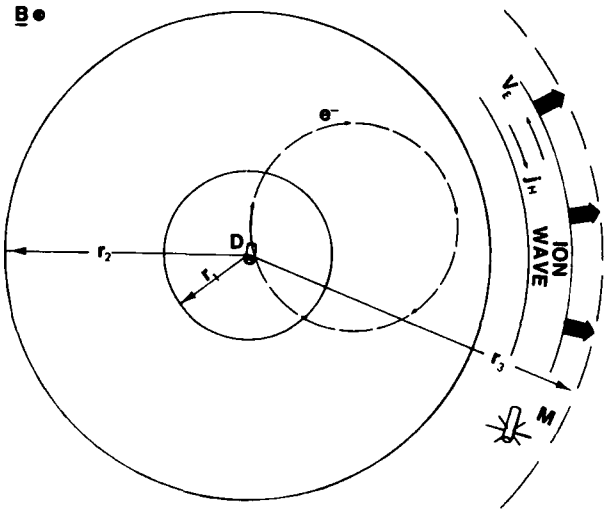

Fig. 7. Ion blast wave model for the MAIMIK experiment. The inner sheath is within r_1, and the quasi-neutral sheath is between r_1 and r_2. The locations for the active daughter and mother are indicated by the letters "D" and "M", respectively. The trajectory for a primary beam electron is also indicated in the figure. The distances are not to scale. As the ion wave passes the position of the mother payload it produces a radial electric field that drives a Hall current $\mathbf{j_H}$ carried by $\mathbf{E} \times \mathbf{B}$ drifting electrons.

The sudden occurrence of $E_\rho(\mathbf{r}', \mathbf{t})$, the radial component of $\mathbf{E}$, in the presence of the downward pointing magnetic field, $\mathbf{B} = \hat{\mathbf{z}}\mathbf{B}$, caused the local electrons to initiate a counterclockwise $\mathbf{E} \times \mathbf{B}$ drift while the more massive background ions remained stationary. The drift motion of the background electron gas in the absence of ion drifts constituted a Hall current of the form

$$\mathbf{J_H}(\mathbf{r}', \mathbf{t}) = -\mathbf{e}\mathbf{n}_\circ\mathbf{V_E}(\mathbf{r}', \mathbf{t}) = -\mathbf{e}\mathbf{n}_\circ\mathbf{E} \times \mathbf{B}/\mathbf{B}^2$$

$$= -(\epsilon_\circ\omega_{pe}^2/\Omega_e)E_\rho(\mathbf{r}', \mathbf{t})\hat{\mathbf{j}}_\phi \quad (1)$$

where $n_\circ$ was the measured ambient plasma density and $\omega_{pe}^2 \equiv (n_\circ e^2/\epsilon_\circ m_e)$ and $\Omega_e \equiv (eB/m_e)$ were, respectively, the electron plasma and electron cyclotron frequencies. The currents carried by the $\mathbf{E} \times \mathbf{B}$ drifting electrons gave rise to a perturbation magnetic field $\delta\mathbf{B}$, whose curl was

$$\nabla \times \delta\mathbf{B} = \mu_\circ\mathbf{J_H}(\mathbf{r}', \mathbf{t}) = (\omega_{pe}^2/\mathbf{c}^2\boldsymbol{\Omega}_e)\mathbf{E}_\rho(\mathbf{r}', \mathbf{t})\hat{\mathbf{j}}_\phi \quad (2)$$

where $c^2 \equiv (\mu_\circ\epsilon_\circ)^{-1}$ was the speed of light. The vector potential $\mathbf{A}$, defined by $\delta\mathbf{B} = \nabla \times \mathbf{A}$, can be substituted into equation (2), yielding

$$\nabla^2\mathbf{A}(\mathbf{r}', \mathbf{t}) = -\mu_\circ\mathbf{J_H}(\mathbf{r}', \mathbf{t}) \quad (3)$$

where a Coulomb gauge, $\nabla \cdot \mathbf{A} = \mathbf{0}$, has been used. The electromagnetic component of the electric field expressed in terms of the vector potential via Faraday's law was

$$\nabla \times \xi(\mathbf{r}, \mathbf{t}) = -\partial\delta\mathbf{B}(\mathbf{r}, \mathbf{t})/\partial\mathbf{t} = -\nabla \times \partial\mathbf{A}(\mathbf{r}, \mathbf{t})/\partial\mathbf{t} \quad (4)$$

or

$$\xi(\mathbf{r}, \mathbf{t}) = -\partial\mathbf{A}(\mathbf{r}, \mathbf{t})/\partial\mathbf{t} \quad (5)$$

The solution to equation (3) for the vector potential at the location of an observer at $\mathbf{r}$ was the weighted integral of the Hall currents over all space,

$$\mathbf{A}(\mathbf{r}, \mathbf{t}) = (\mu_\circ/4\pi)\int \mathbf{d}^3\mathbf{r}'\mathbf{J_H}(\mathbf{r}', \mathbf{t})/\mid \mathbf{r} - \mathbf{r}' \mid \quad (6)$$

where each current element depended only on its local electric field to drive particle motion. A time derivative of equation (6) shows explicitly that the variation in the vector potential at $\mathbf{r}$ was not uniquely dependent upon the local change in $\mathbf{E}$ but might have depended more heavily on the dominant changes in the system. In other words, the causal relationship between the electrostatic and electromagnetic components of $\mathbf{E}$ was not defined at a point but represented the system as a whole.

Our presentation of the blast wave model is overly simplistic in that it has ignored, up to this point, the plasma properties of the medium other than the availability of the space charge. The impulse electric field signature in Figure 3 indicates that the measured fields reflect more local variations in the plasma than the simple blast wave and equation (6) might suggest. That is, the form of the impulse response suggests that the expanding ion cloud was continuously shielded by the background electron gas and that the fields at $\mathbf{r}'$ resulted from a more local variation of η, the space charge density within the ion cloud. Similarly, the neglect of any dielectric and diamagnetic effects which affect electromagnetic wave propagation within the medium limit the applicability of equation (6). An accurate model of the ion cloud kinematics requires a detailed knowledge of the potential distribution within the evolving inner sheath that is beyond the scope of the present work. For the purposes of the present model, however, it is reasonable to assume that the potential decreased monotonically with radius near the daughter payload. The dynamics of the expanding ion cloud would then suggest that the innermost ions gained the greatest kinetic energy and were the first particles to reach the distant radial locations. In time the portion of the cloud that swept past $\mathbf{r}'$ originated at the outer regions of the sheath. The initial unfolding of the inner sheath particles caused a positive gradient in the effective space charge density within the expanding cloud. For $\eta(\mathbf{r}'', \mathbf{t}) > \mathbf{0}$ and $\partial\eta(\mathbf{r}'', \mathbf{t})/\partial\mathbf{r} > \mathbf{0}$ the local (unshielded) contributions to the space charge created an electrostatic field at $\mathbf{r}''$ that was directed out. The rapidly increasing electric field at the head of the ion cloud would tend to drive clockwise directed

electron Hall currents that were the largest contributors to $\partial \mathbf{A}/\partial t$. The resultant deflection for the electromagnetic field by virtue of equation (5) was therefore counterclockwise as measured on MAIMIK.

The blast wave model is also consistent with the observation of the impulse fields only at the initiation of the beam pulse whereas perturbation fields might have been be expected as (1) the expanding ion cloud was swept past the observer, (2) vehicle potential varied due to an oscillating virtual cathode, and (3) at beam termination. However, once the background ions were evacuated from the inner sheath, charge neutrality was ultimately maintained by ambipolar electron flow along magnetic field lines. Since ambipolar diffusion was controlled by the dynamics of the background ions, the associated plasma response time was much slower than the initial expansion rate of the ion cloud. These perturbation fields would be smaller than the initial impulse fields and were apparently below the sensitivity of the MAIMIK instrument.

Finally, we note that the blast wave model is consistent with the observation of a current threshold for the impulse fields. We suspect that the lack of a clear impulse signature for currents below 160 mA was related to the anomalous electron heating effect discussed by Svenes et al. [1988]. Although the smaller currents did not supercharge the daughter payload, the steady state potential of the vehicle was sufficiently large that in the absence of mitigating forces, the ions originally near the charged vehicle should have been accelerated outward. However, the increased mobility of the heated electrons near the active rocket may have sufficiently modified the local potential distribution and minimized the ion acceleration that, in turn, reduced the effects of the ion wave.

Just as the case of the vacuum model, the ion blast wave model alone is inadequate to fully explain the MAIMIK electric field observations. For example, an observational feature of the impulse fields that did not agree with the blast wave model was the upward pointing fields within the 50-m cross-field distance of the central body (Figure 4). We suggest that elements of both the vacuum and ion blast wave models are needed to explain the electric field observations. The blast wave model has been used here to explain (1) the outward pointing fields having consistent tangential deflections at all azimuthal locations for the larger beam currents (Figure 5), (2) the impulse response signature for the beam pulse showing a rapid rise in the amplitude of the field followed by a more gradual decay (Figure 3), (3) the current threshold above 80 mA for the observation of the impulse fields, and (4) the lack of a response field at the termination of the beam and for changes in the potential of the payload following the initial rise. On the other hand, the vacuum model qualitatively described the azimuthal dependence in the amplitude of the radial fields and the upward pointing electric field components along the magnetic field that were measured in the outer sheath region. The explanation of the remote electric field observations may also require an addition source term that is presently unknown. A complete solution to the problem exceeds the limits of the conceptual models presented here and the limits of the data to discern between the models.

CONCLUSIONS

The characteristics of the impulse electric fields measured during supercharging events on the MAIMIK electron beam rocket experiment were consistent with a general model of an outwardly propagating ion blast wave originating within the strong sheath of the charged central body and modified by the electrostatics of the space charges resulting from the virtual cathode and escaping beam. The electric field signatures at distant locations consisted of electrostatic and electromagnetic components that were coupled through the set of Maxwell equations. The radial electrostatic fields were caused by the net space charge carried by the ions blast wave. The azimuthal dependence in the amplitude of the radial fields was, perhaps, due to variations in the charge density in the ion blast wave that in turn may have been influenced by the initial space charge distribution of the virtual cathode near the active payload. The tangential electromagnetic components were generated by the $\mathbf{E} \times \mathbf{B}$ drift response of the cold background electrons at the front of the wave.

The ion blast wave model depends critically upon the rapid acceleration and outward propagation of the background ions near the beam-emitting payload. The measurement of the energetic ion flux and the probable interpretation provided by *Kellogg and Monson* [1988] are consistent with this model. However, these measurements only confirm the initial premise of the blast wave model, that is, ion acceleration near the rocket body. The blast wave model attempts to describe a more subtle interaction between the outward propagating ion cloud and the local ionosphere in terms of the plasma shielding effects and the coupling of the electrostatic and electromagnetic components of the electric fields. Clearly, the shortcomings of the model are its inability of accurately accounting for the magnitudes of the radial field components and the orientation of the axial field at all distances. Some of these deficiencies can be reduced by considering a model that combines a initial vacuum solution with the ion blast wave model.

Acknowledgments. This work was begun while N.C.M. was an employee of NASA Goddard Space Flight Center. The experiment was jointly sponsored by NASA and the Royal Norwegian Council for Scientific and Industrial Research. The analysis effort at the Geophysics Laboratory was supported by program element 62101F, project 7601, and by the Air Force Office of Scientific Research under program element 61102F, tasks 2311G5 and 2311G6. Useful discussions with D. Cooke, G. Ginet, M. Heinemann, F. Rich, J. Troim, and J. Winckler are acknowledged.

The Editor thanks T. Neubert and K. N. Erickson for their assistance in evaluating this paper.

REFERENCES

Bering, E. A., A sounding rocket observation on an apparent wake generated parallel electric field, *J. Geophys. Res.*, *88*, 961-979, 1983.

Borovsky, J. E., The dynamic sheath: Objects coupling to plasmas on electron-plasma-frequency time scales, *Phys. Fluids*, *31*, 1074-1100, 1988.

Cambou, F., V. S. Dokoukine, V. N. Ivchenko, G. G. Managadze, V. V. Migulin, O. K. Nazarenko, A. T. Nesmyanovich, A. K. Pyatsi, R. Z. Sagdeev, and I. A. Zhulin, The Zarnitza Rocket experiment on electron injection, *Space Res.*, *15*, 491-500 ,1975.

Cooke, D. L. and I. Katz, Ionization-induced instability in an electron-collecting sheath, *J. Spacecr. Rockets*, *25*, 132-138, 1988.

Erickson, K. N., and J. R. Winckler, A study of plasma heating, electric fields and plasma flow near an electron beam-emitting rocket system in the polar ionosphere, *Cosmic Phys. Tech. Rep.*, *201*, 55 pp., Univ. of Minn., Minneapolis, 1988.

Grandal, B. (Ed.), *Artificial Particle Beams in Space Plasma Studies*, 704 pp., Plenum, New York, 1982.

Hendrickson, R. A., R. W. McEntire, and J. R. Winckler, Electron echo experiment: A new magnetospheric probe, *Nature*, *230*, 564-566, 1971.

Hess, W. N., M. C. Trichel, T. N. Davis, W. C. Beggs, G. E. Kraft, E. Stassinopoulos, and E. J. R. Maier, Artificial auroral experiment: Experiment and principal results, *J. Geophys. Res.*, *76*, 6067-6081, 1971.

Jacobsen, T. A., and N. C. Maynard, POLAR 5 - An electron accelerator experiment within an aurora, 3, Evidence for significant spacecraft charging by an electron accelerator at ionospheric altitudes, *Planet. Space Sci.*, *28*, 291-307, 1980.

Kellogg, P. J., and S. J. Monson, Charging and the cross-field discharge during electron accelerator operation on a rocket, *J. Geomagn. Geoelectr.*, *40*, 1257-1267, 1988.

Maehlum, B. N., Beam-plasma experiments, *Comput. Phys. Commun.*, *49*, 119-132, 1988.

Maehlum, B. N., W. F. Denig, A. A. Egeland, M. Friedrich, T. Hansen, G. K. Holmgren, K. Maseide, N. C. Maynard, B. T. Narheim, K. Svenes, K. Torkar, J. Troim, and J. D. Winningham, MAIMIK - A high current electron beam experiment on a sounding rocket from Andoya rocket range, *Eur. Space Agency Spec. Publ., ESA SP-270*, 261-265, 1987.

Maehlum, B. N., J. Troim, N. C. Maynard, W. F. Denig, M. Friedrich, and K. M. Torkar, Studies of the electrical charging of the tethered electron accelerator mother-daughter rocket MAIMIK, *Geophys. Res. Lett.*, *15*, 725-728, 1988.

Maehlum, B. N., M. Friedrich, W. F. Denig, G. Holmgren, N. C. Maynard, W. J. Burke, K. Svenes, K. M. Torkar, and J. Troim, MAIMIK - A tethered "mother-daughter" electron accelerator rocket, *Adv. Space Res.*, *10*, (7)125-(7)132, 1990.

Managadze, G. G., W. K. Riedler, M. F. Friedrich, V. M. Balebanov, A. A. Lalaishvili, N. A. Leonov, S. B. Lyakhov, A. A. Martinson, A. D. Mayorov, Z. Klos, Z. Zbyszynski, and K. M. Torkar, Potential observations of an electron emitting rocket payload and other related plasma measurements, *Planet. Space Sci.*, *36*, 399-410, 1988.

Mandell, M. J., I. Katz, and D. L. Cooke, Numerical simulation of vehicle charging in excess of the beam energy by an intense electron beam (abstract), *Eos Trans. AGU*, *69*, 1371, 1988.

Maynard, N. C., D. S. Evans, and J. Troim, Electric field observations of time constants related to charging and charge neutralization processes in the ionosphere, in *Artificial Particle Beams in Space Plasma Studies*, edited by B. Grandal, pp. 627-644, Plenum, New York, 1982.

Miller, R. B., *An Introduction to the Physics of Intense Charged Particle Beams*, 351 pp., Plenum, New York, 1982.

Myers, N. B., W. J. Raitt, B. E. Gilchrist, P. M. Banks, T. Neubert, P. R. Williamson, and S. Sasaki, A comparison of current-voltage relationships of collectors in the Earth's ionosphere with and without electron beam emission, *Geophys. Res. Lett.*, *16*, 365-368, 1989.

Myers, N. B., W. J. Raitt, A. B. White, P. M. Banks, B. E. Gilchrist, and S. Sasaki, Vehicle charging effects during electron beam emission from the CHARGE-2 experiment, *J. Spacecr. Rockets*, *27*, 25-37, 1990.

Parker, L. W., and B. L. Murphy, Potential buildup on an electron-emitting ionospheric satellite, *J. Geophys. Res.*, *72*, 1631-1636, 1967.

Singh, N., and K. S. Hwang, Electrostatic charging of spacecraft in response to electron beam injection, *Phys. Scr.*, *40*, 295-301, 1989.

Steinberg, J. T., D. A. Gurnett, P. M. Banks, and W. J. Raitt, Double-probe potential measurements near the Spacelab 2 electron beam, *J. Geophys. Res.*, *93*, 10001-10010, 1988.

Svenes, K., J. Troim, M. Friedrich, K. M. Torkar, and G. Holmgren, Ionospheric plasma measurements from the accelerator rocket MAIMIK, *Planet. Space Sci.*, *36*, 1509-1522, 1988.

Svenes, K. R., J. Troim, B. N. Maehlum, M. Friedrich, K. M. Torkar, G. Holmgren, and W. F. Denig, Ram-wake measurements obtained from the ionospheric sounding rocket MAIMIK, *Planet. Space Sci.*, *38*, 653-663, 1990.

Syvertsen, R., Electron accelerator documentation, *Rep. FFI/NOTAT-85/7046*, 37 pp., Norw. Def. Res. Estab., Kjeller, Norway, 1985.

Szuszczewicz, E. P., Controlled electron beam experiments in space and supporting laboratory experiments: A review, *J. Atmos. Terr. Phys.*, *47*, 1189-1210, 1985.

Winckler, J. R., The application of artificial electron beams to magnetospheric research, *Rev. Geophys., Space Phys.*, *18*, 659-682, 1980.

Winckler, J. R., P. R. Malcolm, R. L. Arnoldy, W. J. Burke, K. N. Erickson, J. Ernstmeyer, R. C. Franz, T. J. Hallinan, P. J. Kellogg, S. J. Monson, K. A. Lynch, G. Murphy, and R. J. Nemzek, ECHO 7 - An electron beam experiment in the magnetosphere, *Eos Trans. AGU*, *70*, 657-668, 1989.

Winglee, R. M., and P. L. Pritchett, Comparative study of cross-field and field-aligned electron beams in active experiments, *J. Geophys. Res.*, *93*, 5823-5844, 1988.

W. J. Burke, W. F. Denig, and N. C. Maynard, Space Physics Division, Geophysics Laboratory (AFSC), Hanscom Air Force Base, Bedford, MA 01731-5000

B. N. Maehlum, Norwegian Defence Research Establishment, N-2007 Kjeller, Norway.

(Received December 27, 1989;
revised August 13, 1990;
accepted August 27, 1990.)